

CoDiCast: Conditional Diffusion Model for Global Weather Prediction with Uncertainty Quantification

Jimeng Shi¹, Bowen Jin², Jiawe Han², Sundararaman Gopalakrishnan³, Giri Narasimhan¹

¹Florida International University,

²University of Illinois Urbana-Champaign,

³Hurricane Research Division, National Oceanic and Atmospheric Administration

{jshi008, giri}@fiu.edu, {bowenj4, hanj}@illinois.edu

sundararaman.g.gopalakrishnan@noaa.gov

ABSTRACT

Accurate weather forecasting is critical for science and society. However, existing methods have not achieved the combination of high accuracy, low uncertainty, and high computational efficiency simultaneously. On one hand, traditional numerical weather prediction (NWP) models are computationally intensive because of their complexity. On the other hand, most machine learning-based weather prediction (MLWP) approaches offer efficiency and accuracy but remain deterministic, lacking the ability to capture forecast uncertainty. To tackle these challenges, we propose a conditional diffusion model, CoDiCast, to generate global weather prediction, integrating accuracy and uncertainty quantification at a modest computational cost. The key idea behind the prediction task is to generate realistic weather scenarios at a *future* time point, conditioned on observations from the *recent past*. Due to the probabilistic nature of diffusion models, they can be properly applied to capture the uncertainty of weather predictions. Therefore, we accomplish uncertainty quantifications by repeatedly sampling from stochastic Gaussian noise for each initial weather state and running the denoising process multiple times. Experimental results demonstrate that CoDiCast outperforms several existing MLWP methods in accuracy, and is faster than NWP models in the inference speed. Our model can generate 6-day global weather forecasts, at 6-hour steps and 5.625° latitude-longitude resolutions, for over 5 variables, in about 12 minutes on a commodity A100 GPU machine with 80GB memory. Our code is available at <https://github.com/JimengShi/CoDiCast>.

1 INTRODUCTION

Weather prediction describes how the weather states evolve by mapping the current weather states to future weather states (Palmer, 2012). Accurate weather forecasting is crucial for a wide range of societal activities, from daily planning to disaster preparedness (Merz et al., 2020; Shi et al., 2024). For example, governments, organizations, and individuals rely heavily on weather forecasts to make informed decisions that can significantly impact safety, economic efficiency, and overall well-being. However, weather predictions are intrinsically uncertain largely due to the complex and chaotic nature of atmospheric processes (Slingo & Palmer, 2011). Therefore, assessing the range of probable weather scenarios is significant, enabling informed decision-making.

Traditional numerical weather prediction (NWP) methods achieve weather forecasting by approximately solving the differential equations representing the integrated system between the atmosphere, land, and ocean (Price et al., May 2024; Nguyen et al., 2023). However, running such an NWP model can produce only one possibility of the forecast, which ignores the weather uncertainty. To solve this problem, *Ensemble forecast*¹ of multiple models is often employed to model the probability distribution of different future weather scenarios (Palmer, 2019; Leinonen et al., 2023). While such

¹Generating a set of forecasts, each of which represents a single possible scenario.

NWP-based ensemble forecasts effectively model the weather uncertainty, physics-based models inherently make restrictive assumptions of atmospheric dynamics, and running multiple NWP models requires extreme computational costs (Rodwell & Palmer, 2007).

In recent years, machine learning (ML)-based weather predictions (MLWP) have been proposed to challenge NWP-based prediction methods (Ben Bouallègue et al., 2024; Bülte et al., 2024). They have achieved enormous success with comparable accuracy and a much (usually three orders of magnitude) lower computational overhead. They are typically trained to learn weather patterns from a huge amount of historical data and predict the mean of the probable trajectories by minimizing the mean squared error (MSE) of model forecasts (Hewage et al., 2021). Representative work includes Pangu (Bi et al., 2023), GraphCast (Lam et al., 2023), ClimaX (Nguyen et al., 2023), ForeCastNet (Pathak et al., 2022), Fuxi (Chen et al., 2023b), Fengwu and (Chen et al., 2023a). Despite the notable achievements of these MLWP methods, most of them are deterministic (Kochkov et al., 2024), falling short in capturing the uncertainty in weather forecasts (Jaseena & Kovoov, 2022).

To compute the uncertainty for ML models, two methods exist. Perturbing initial conditions (Morley et al., 2018) helps estimate the aleatoric uncertainty (data noise), while the Monte Carlo Dropout approach (Gal & Ghahramani, 2016) estimates epistemic uncertainty (model uncertainty) (Siddique et al., 2022). However, neither approach fully captures uncertainty in both the input conditions and the evolution of weather models. Additionally, these methods require manual tuning of perturbations and dropout rates, which can negatively impact model accuracy. These limitations motivate us to explore an approach for comprehensive uncertainty quantification without the loss of accuracy.

Denoising probabilistic diffusion models (DDPMs) (Ho et al., 2020) stand out as a probabilistic type of generative models, which can generate high-quality images. By explicitly and iteratively modeling the noise additive and its removal, DDPMs can capture intricate details and textures of images. Furthermore, controllable diffusion models (Rombach et al., 2022; Zhang et al., 2023) enable the generation process to be guided by specific attributes or conditions, e.g., class labels, textual descriptions, or other auxiliary information. By doing so, the models can generate images that adhere to the specified conditions. This inspires us to consider the weather “prediction” tasks as “generation” tasks - generating plausible weather scenarios with conditional diffusion models. Promising potentials could be the following: (1) Weather numerical data is usually a 2-D grid over latitude and longitude, sharing a similar modality with the image. Diffusion models can capture the intricate weather distribution with iterative denoising. (2) Weather states from the recent past (i.e., initial conditions) can be injected into diffusion models to guide the generation of future weather evolution. (3) More notably, the starting noise sampling from the Gaussian distribution can mimic the aleatoric uncertainty while iteratively adding and removing noise captures the epistemic uncertainty. These features prompt probabilistic diffusion models to generate a set of diverse weather scenarios rather than a single deterministic one. This capability makes them well-suited for modeling the uncertain nature of weather evolution. Our contributions are presented as follows:

- We identify the shortcomings of current weather prediction methods. NWP-based methods are limited to restrictive assumptions and computationally intensive. Moreover, a single deterministic NWP- and MLWP-based method cannot achieve uncertainty quantification.
- To address these problems, we propose CoDiCast, a conditional diffusion model for global weather prediction conditioning on observations from the recent past while probabilistically modeling the uncertainty. In addition, we use the cross-attention mechanism to effectively integrate conditions into the denoising process to guide the generation tasks.
- We conduct extensive experiments on a decade of ERA5 reanalysis data from the European Centre for Medium-Range Weather Forecasts (ECMWF), and evaluate our method against several state-of-the-art models in terms of accuracy, efficiency, and uncertainty. It turns out that CoDiCast achieves an essential trade-off among these valuable properties.

2 PRELIMINARIES

In this section, we introduce the problem formulation of global weather prediction and briefly review Denoising Diffusion Probabilistic Models (DDPMs) (Ho et al., 2020).

2.1 PROBLEM FORMULATION

Deterministic Global Weather Predictions. Given the input consisting of the weather state(s), $X^t \in \mathbb{R}^{H \times W \times C}$ at time t , the problem is to predict a point-valued weather state, $X^{t+\Delta t} \in \mathbb{R}^{H \times W \times C}$ at a future time point $t + \Delta t$. $H \times W$ refers to the spatial resolution of data which depends on how densely we grid the globe over latitudes and longitudes, C refers to the number of channels (i.e., weather variables), and the superscripts t and $t + \Delta t$ refer to the current and future time points. The long-range multiple-step forecasts could be achieved by autoregressive modeling or direct predictions.

Probabilistic Global Weather Predictions. Unlike the deterministic models that output point-valued predictions, probabilistic methods model the probability of future weather state(s) as a distribution $P(X^{t+\Delta t} | X^t)$, conditioned on the state(s) from the recent past. Probabilistic predictions are appropriate for quantifying the forecast uncertainty and making informed decisions.

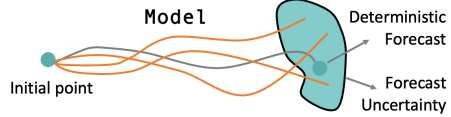


Figure 1: Deterministic vs Probabilistic.

2.2 DENOISING DIFFUSION PROBABILISTIC MODELS

A denoising diffusion probabilistic model (DDPM) (Ho et al., 2020) generates target samples by learning a distribution $p_\theta(x_0)$ that approximates the target distribution $q(x_0)$. DDPM comprises a *forward diffusion* process and a *reverse denoising* process. The *forward process* transforms an input x_0 with a data distribution of $q(x_0)$ to a Gaussian noise vector x_N in N diffusion steps. It can be described as a Markov chain that gradually adds Gaussian noise to the input according to a variance schedule $\{\beta_1, \dots, \beta_N\}$:

$$q(x_n | x_{n-1}) = \mathcal{N}\left(x_n; \sqrt{1 - \beta_n}x_{n-1}, \beta_n \mathbf{I}\right), \text{ and} \quad (1)$$

$$q(x_{1:N} | x_0) = \prod_{n=1}^N q(x_n | x_{n-1}), n \in [1, N], \quad (2)$$

where at each step n , the diffused sample x_n is obtained from x_{n-1} as described above. Multiple steps of the forward process can be described as follows in a closed form:

$$q(x_n | x_0) = \mathcal{N}\left(x_n; \sqrt{\bar{\alpha}_n}x_0, (1 - \bar{\alpha}_n)\mathbf{I}\right),$$

where $\alpha_n = 1 - \beta_n$ and $\bar{\alpha}_n = \prod_{s=1}^n \alpha_s$. Thus, $x_n = \sqrt{\bar{\alpha}_n}x_0 + \sqrt{1 - \bar{\alpha}_n}\epsilon$, with ϵ sampled from $\mathcal{N}(\mathbf{0}, \mathbf{I})$.

In the *reverse process*, the *denoiser* network is used to recover x_0 by stepwise denoising starting from the pure noise sample, x_N . This process is formally defined as:

$$p_\theta(x_{0:N}) = p(x_N) \prod_{n=1}^N p_\theta(x_{n-1} | x_n), \quad (3)$$

where $p_\theta(x_n)$ is the distribution at step n parameterized by θ .

For each iteration, $n \in [1, N]$, diffusion models are trained to minimize the following KL-divergence:

$$\mathcal{L}_n = D_{KL}(q(x_{n-1} | x_n) || p_\theta(x_{n-1} | x_n)). \quad (4)$$

where $q(x_{n-1}|x_n)$ can be computed from $q(x_n|x_{n-1})$ using Bayes rule and the multistep forward process equation above.

3 METHODOLOGY

This section introduces our approach for global weather prediction, CoDiCast, implemented as a conditional diffusion model. The key idea is to consider “prediction” tasks as “generation” tasks while conditioning on the context guidance of past observation(s). An overview of the proposed CoDiCast is shown in Figure 2.

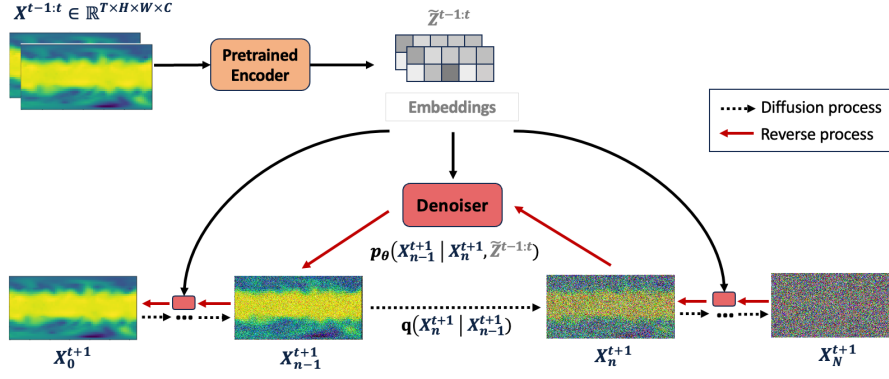


Figure 2: Framework of CoDiCast for global weather forecast. The superscript T and the subscript N denote the time point and iteration step of adding/denoising noise. H and W represent the height (#latitude) and width (#longitude) of grid data. C is the number of variables of interest.

3.1 FORWARD DIFFUSION PROCESS

The forward diffusion process is straightforward. Assuming the current time point is t , for the sample at time point $t + 1$, $X_0^{t+1} \in \mathbb{R}^{H \times W \times C}$, which is of interest to predict, we first compute the diffused sample by gradually adding noise until the N^{th} iteration (see the dotted lines in Figure 2):

$$X_n^{t+1} = \sqrt{\bar{\alpha}_n} \cdot X_0^{t+1} + \sqrt{1 - \bar{\alpha}_n} \epsilon, \quad (5)$$

where ϵ is sampled from $\mathcal{N}(\mathbf{0}, \mathbf{I})$ with the same size as X_0^{t+1} , and $\bar{\alpha}$ is same as that in Eq. (2.2).

3.2 REVERSE CONDITIONAL DENOISING PROCESS

CoDiCast models the probability distribution of the future weather state conditioning on the current and previous weather states. More specifically, we exploit a pre-trained encoder to learn conditions as embedding representations of the past observations X^{t-1} and X^t , which are used to control and guide the synthesis process. Compared to modeling the past observations in the original space, we found that our embedding representations in the latent space work better.

$$p_\theta(X_{0:N}^{t+1} | \tilde{Z}^{t-1:t}) = p(X_N^{t+1}) \prod_{n=1}^N p_\theta(X_{n-1}^{t+1} | X_n^{t+1}, \tilde{Z}^{t-1:t}), \quad (6)$$

where $X_N^{t+1} \sim \mathcal{N}(\mathbf{0}, \mathbf{I})$, $\tilde{Z}^{t-1:t}$ is the embedding representation as shown in Eq. (8).

After prediction at the first time point is obtained, a forecast trajectory, $X^{1:T}$, of length T , can be auto-regressively modeled by conditioning on the predicted ‘‘previous’’ states.

$$p_\theta(X_{0:N}^{1:T}) = \prod_{t=1}^T p(X_N^t) \prod_{n=1}^N p_\theta(X_{n-1}^t | X_n^t, \tilde{Z}^{t-2:t-1}). \quad (7)$$

3.3 PRE-TRAINED ENCODER

We learn an encoder by training an autoencoder network (Baldi, 2012). An Encoder compresses the input at each time point into a latent-space representation, while Decoder reconstructs the input from the latent representation. After the encoder, \mathcal{F} , is trained, it can serve as a pre-trained representation learning model to project the original data into latent embedding in Eq. (8). Appendix B.1 provides more details.

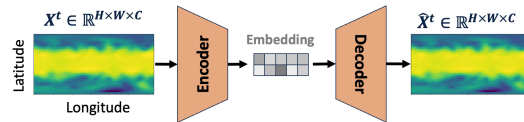


Figure 3: Autoencoder structure.

$$\tilde{Z}^{t-1:t} = \mathcal{F}(X^{t-1}, X^t) \quad (8)$$

3.4 ATTENTION-BASED DENOISER NETWORK

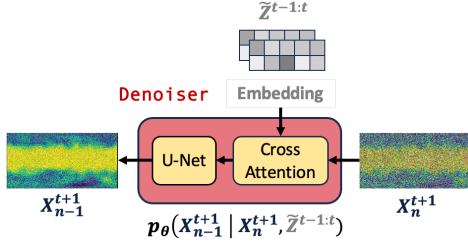


Figure 4: Attention-based denoiser structure.

Our denoiser network consists of two blocks: cross-attention and U-net (as shown in Figure 4). Cross-attention mechanism (Hertz et al., 2022) is employed to capture how past observations can contribute to the generation of future states. The embedding of past observations, $\tilde{Z}^{t-1:t}$, and the noise data X_n^{t+1} at diffusion step n , are projected to the same hidden dimension d with the following transformation:

$$Q = W_q \cdot X_n^{t+1}, K = W_k \cdot \tilde{Z}^{t-1:t}, V = W_v \cdot \tilde{Z}^{t-1:t}, \quad (9)$$

where $X_n^{t+1} \in \mathbb{R}^{(H \times W) \times C}$ and $\tilde{Z}^{t-1:t} \in \mathbb{R}^{(H \times W) \times d_z}$. $W_q \in \mathbb{R}^{d \times C}$, $W_k \in \mathbb{R}^{d \times d_z}$, $W_v \in \mathbb{R}^{d \times d_z}$ are learnable projection matrices (Vaswani et al., 2017). Then we implement the cross-attention mechanism by $\text{Attention}(Q, K, V) = \text{softmax}(\frac{QK^T}{\sqrt{d}})V$. A visual depiction of the cross-attention mechanism is in Appendix B.2.

U-Net (Ronneberger et al., 2015) is utilized to recover the data by removing the noise added at each diffusion step. The *skip connection* technique in U-Net concatenates feature maps from the encoder to the corresponding decoder layers, allowing the network to retain fine-grained information that might be lost during downsampling. The detailed U-Net architecture is presented in Appendix B.3.

3.5 TRAINING PROCESS

The training procedure is shown in Algorithm 1. Firstly, we pre-train an encoder to learn the condition embedding of the past observations. Subsequently, we inject it into our conditional diffusion model and train CoDiCast with the devised loss function:

$$\mathcal{L}_{cond}(\theta) = \mathbb{E}_{X_0, \epsilon, n} \|\epsilon - \epsilon_\theta(X_n^{t+1}, n, \text{cond})\|^2, \quad (10)$$

where $X_n^{t+1} = \sqrt{\alpha_n}X_0^{t+1} + \sqrt{1 - \alpha_n}\epsilon$, $\text{cond} = \mathcal{F}(X^{t-1:t})$, and ϵ_θ is the denoiser in Figure 4.

3.6 INFERENCE PROCESS

Algorithm 2 describes the inference process. We first extract the conditional embedding representations, $\tilde{Z}^{t-1:t}$, by the pre-trained encoder, and then randomly generate a noise vector $X_N \sim \mathcal{N}(\mathbf{0}, \mathbf{I})$ of size $H \times W \times C$. The sampled noise vector, X_N , is autoregressively denoised along the reversed chain to predict the target until n equals 1 (ζ is set to zero when $n = 1$), we obtain weather prediction \hat{X}_0 at the time $t + 1$. Later, multi-step prediction can be implemented autoregressively - the output from the previous time step is the input while predicting the next step, as shown in Eq. (7).

Algorithm 1 Training

- 1: **Input:** Number of diffusion steps N , pre-trained encoder \mathcal{F}
- 2: **Output:** Trained denoising function $\epsilon(\cdot)$
- 3: **repeat**
- 4: $X_0^{t+1} \sim q(X_0^{t+1})$
- 5: $n \sim \text{Uniform}(1, 2, \dots, N)$
- 6: $\epsilon \sim \mathcal{N}(\mathbf{0}, \mathbf{I})$
- 7: Get the past observations X^{t-1}, X^t
- 8: Get embedding $\tilde{Z}^{t-1:t} = \mathcal{F}(X^{t-1}, X^t)$
- 9: Take gradient descent step on:

$$\nabla_\theta \|\epsilon - \epsilon_\theta(X_n^{t+1}, n, \tilde{Z}^{t-1:t})\|^2$$

- 10: **until** converged
-

Algorithm 2 Inference

- 1: **Input:** Number of diffusion steps N , pre-trained encoder \mathcal{F} , trained denoising network $\epsilon(\cdot)$, past observations X^{t-1}, X^t
 - 2: **Output:** Inference target X_0^{t+1}
 - 3: Get embedding $\tilde{Z}^{t-1:t} = \mathcal{F}(X^{t-1}, X^t)$
 - 4: $X_N \sim \mathcal{N}(\mathbf{0}, \mathbf{I})$
 - 5: **for** $n = N, \dots, 1$ **do**
 - 6: $\zeta \sim \mathcal{N}(\mathbf{0}, \mathbf{I})$ if $n \geq 1$, else $\zeta = 0$
 - 7: $X_{n-1}^{t+1} = \frac{1}{\sqrt{\alpha_n}} \left(X_n^{t+1} - \frac{1 - \alpha_n}{\sqrt{1 - \alpha_n}} \epsilon_\theta(X_n^{t+1}, n, \tilde{Z}^{t-1:t}) \right) + \sigma_n \zeta$
 - 8: **end for**
 - 9: **return** X_0^{t+1}
-

3.7 ENSEMBLE FORECAST

To enhance the reliability of weather forecasts, *ensemble forecast* strategy is often employed to capture the variability among forecasts by separately running multiple deterministic models, e.g., ensemble forecast suite (ENS) (Buizza, 2008). In our approach, since CoDiCast is a probabilistic model that can generate a distribution of future weather scenarios rather than a single prediction, following (Price et al., May 2024), we run the trained CoDiCast multiple times to get the ensemble instead. More specifically, by integrating both initial conditions and noise sampled from a Gaussian distribution, CoDiCast implements the ensemble forecast through multiple stochastic samplings during inference, capturing a range of possible forecasts for the uncertainty quantification.

4 EXPERIMENTS

4.1 DATASET AND BASELINES

Dataset. ERA5 (Hersbach et al., 2020) is a publicly available atmospheric reanalysis dataset provided by the European Centre for Medium-Range Weather Forecasts (ECMWF). Following the existing work (Verma et al., 2024), we use the preprocessed 5.625° resolution (32×64) and 6-hour increment ERA5 dataset from WeatherBench (Rasp et al., 2020). We downloaded 5 variables for the globe: geopotential at 500 hPa pressure level (Z500), atmospheric temperature at 850 hPa pressure level (T850), ground temperature (T2m), 10 meter U wind component (U10) and 10 meter V wind component (V10). More details can be found in Table 3 in Appendix A.

Baselines. We comprise the following baselines: ClimODE (Verma et al., 2024): a spatiotemporal continuous-time model that incorporates the physic knowledge of atmospheric *advection* over time; ClimaX (Nguyen et al., 2023): a state-of-the-art vision Transformer-based method trained on the same dataset (without pre-training that is used in the original paper); FourCastNet (Pathak et al., 2022): a global data-driven weather model using adaptive Fourier neural operators; Neural ODE (Chen et al., 2018): an ODE network that learns the time derivatives as neural networks by solving an ordinary differential equation; Integrated Forecasting System IFS (Rasp et al., 2020): a global numerical weather prediction (NWP) system, integrating multiple advanced physics-based models to deal with more meteorological variables across multiple altitudes. Our study focuses solely on a subset of these variables due to the limited computational resources, with IFS serving as the gold standard. For a fair comparison, all ML models use the same data set described in Section 4.1.

4.2 EXPERIMENTS DESIGN

We use data between 2006 and 2015 as the training set, data in 2016 as the validation set, and data between 2017 and 2018 as the testing set. We assess the global weather forecasting capabilities of our method CoDiCast by predicting the weather at a future time $t + \Delta t$ ($\Delta t = 6$ to 144 hours) based on the past two time units. To quantify the uncertainty in weather prediction, we generate an “ensemble” forecast by running CoDiCast five times during the inference phase.

Training. We first pretrain an `encoder` with the `Autoencoder` architecture. For the diffusion model, we used U-Net as the denoiser network with 1000 diffusion/denoising steps. The architecture is similar to that of DDPM (Ho et al., 2020) work. We employ four U-Net units for both the downsampling and upsampling processes. Before training, we apply Max-Min normalization (Ali et al., 2014) to scale the input data within the range $[0, 1]$, mitigating potential biases stemming from varying scales (Shi et al., 2023). Adam was used as the optimizer, where the learning rate $= 2e^{-4}$, decay steps $= 10000$, decay rate $= 0.95$. The batch size and number of epochs were set to 64 and 800 respectively. More training details and model configurations are in Appendix C.

Evaluation Metrics. Following (Verma et al., 2024), we use latitude-weighted Root Mean Square Error (RMSE) and Anomaly Correlation Coefficient (ACC) as deterministic metrics. RMSE measures the average difference between values predicted by a model and the actual values. ACC is the correlation between prediction anomalies relative to climatology and ground truth anomalies relative to climatology. It is a critical metric in climate science to evaluate the model’s performance in capturing unusual weather or climate events. Appendix D contains the formulas of these metrics.

4.3 QUANTITATIVE EVALUATION

Accuracy. We compare different models in forecasting five primary meteorological variables as described in Section 4.1. Table 1 shows that CoDiCast presents superior performance over other MLWP baselines in terms of RMSE and ACC metrics, demonstrating diffusion models can capture the weather dynamics and make predictions accurately. However, there is still room for CoDiCast to be improved compared with the gold-standard IFS model which integrates more meteorological variables.

Table 1: Latitude-weighted RMSE (\downarrow) and ACC (\uparrow) comparison on global weather forecasting. The results of NODE, ClimaX, and ClimODE models are from the ClimODE paper (Verma et al., 2024). N/A represents the values that are not available from their paper. ForeCastNet was re-trained with their code (Pathak et al., 2022). We employ the Monte Carlo Dropout approach (Gal & Ghahramani, 2016) during the inference to compute the uncertainty. We mark the scores in **bold** if our model CoDiCast performs the best among MLWP methods.

Variable	Lead time (Hours)	RMSE (\downarrow)						ACC (\uparrow)					
		NODE	ClimaX	ForeCastNet	ClimODE	CoDiCast	IFS	NODE	ClimaX	ForeCastNet	ClimODE	CoDiCast	IFS
Z500	6	300.6	247.5	222.7±18.1	102.9±9.3	73.1±6.7	26.9	0.96	0.97	0.97	0.99	0.99	1.00
	12	460.2	265.3	310.9±22.7	134.8±12.3	114.2±8.9	33.8	0.88	0.96	0.95	0.99	0.99	0.99
	24	877.8	364.9	402.6±27.3	193.4±16.3	186.5±11.8	51.0	0.70	0.93	0.92	0.98	0.98	0.99
	72	N/A	687.0	755.3±45.8	478.7±48.5	451.6±39.5	123.2	N/A	0.73	0.75	0.88	0.92	0.98
	144	N/A	801.9	956.1±59.1	783.6±37.3	757.5±42.8	398.7	N/A	0.58	0.64	0.61	0.78	0.86
T850	6	1.82	1.64	1.75±0.16	1.16±0.06	1.02±0.05	0.69	0.94	0.94	0.94	0.97	0.99	0.99
	12	2.32	1.77	2.15±0.20	1.32±0.13	1.26±0.10	0.75	0.85	0.93	0.92	0.96	0.99	0.99
	24	3.35	2.17	2.51±0.27	1.55±0.18	1.52±0.16	0.87	0.72	0.90	0.89	0.95	0.97	0.99
	72	N/A	3.17	3.69±0.34	2.58±0.16	2.54±0.14	1.15	N/A	0.76	0.77	0.85	0.93	0.96
	144	N/A	3.97	4.29±0.42	3.62±0.21	3.61±0.19	2.23	N/A	0.69	0.71	0.77	0.85	0.81
T2m	6	2.72	2.02	2.05±0.18	1.21±0.09	0.95±0.07	0.69	0.82	0.92	0.94	0.97	0.99	0.99
	12	3.16	2.26	2.49±0.21	1.45±0.10	1.21±0.07	0.77	0.68	0.90	0.92	0.96	0.99	0.99
	24	3.86	2.37	2.78±0.26	1.40±0.09	1.45±0.07	1.02	0.79	0.89	0.91	0.96	0.99	0.99
	72	N/A	2.87	3.77±0.32	2.75±0.49	2.39±0.37	1.26	N/A	0.83	0.85	0.85	0.96	0.96
	144	N/A	3.38	4.39±0.41	3.30±0.23	3.45±0.22	1.78	N/A	0.83	0.81	0.79	0.91	0.82
U10	6	2.30	1.58	1.98±0.17	1.41±0.07	1.24±0.06	0.61	0.85	0.92	0.87	0.91	0.95	0.98
	12	3.13	1.96	2.58±0.21	1.81±0.09	1.50±0.08	0.76	0.70	0.88	0.78	0.89	0.93	0.98
	24	4.10	2.49	3.02±0.27	2.01±0.10	1.87±0.09	1.11	0.50	0.80	0.71	0.87	0.89	0.97
	72	N/A	3.70	4.17±0.36	3.19±0.18	3.15±0.19	1.57	N/A	0.45	0.41	0.66	0.71	0.94
	144	N/A	4.24	4.63±0.45	4.02±0.12	4.25±0.15	3.04	N/A	0.30	0.28	0.35	0.42	0.72
V10	6	2.58	1.60	2.16±0.19	1.53±0.08	1.30±0.06	0.61	0.81	0.92	0.86	0.92	0.95	1.00
	12	3.19	1.97	2.73±0.23	1.81±0.12	1.56±0.09	0.79	0.61	0.88	0.76	0.89	0.93	0.99
	24	4.07	2.48	3.15±0.28	2.04±0.10	1.94±0.14	1.33	0.35	0.80	0.68	0.86	0.89	1.00
	72	N/A	3.80	4.26±0.34	3.30±0.22	3.18±0.19	1.67	N/A	0.39	0.38	0.63	0.68	0.93
	144	N/A	4.42	4.64±0.45	4.24±0.10	4.21±0.18	3.26	N/A	0.25	0.27	0.32	0.37	0.71

Uncertainty. The gray-shaded error range in Table 1 represents model uncertainty, with fluctuations remaining within 10% of the ground truth scale. This indicates the robustness of ML models. However, ForeCastNet predictions fluctuate relatively larger due to the sensitive selection of the dropout rate. We provide a case study of CoDiCast forecast for 72 hours with uncertainty quantification in Figure 5. It shows the mean prediction tracks the general trend of the ground truth and the uncertainty grows as the lead time increases. The increasing uncertainty over time aligns with the common intuition that longer forecasting horizons make time series predictions more challenging. Besides, we can tell that most actual values fall within the 1 or 2 standard deviations (σ) ranges, indicating these predictions are reasonably accurate.

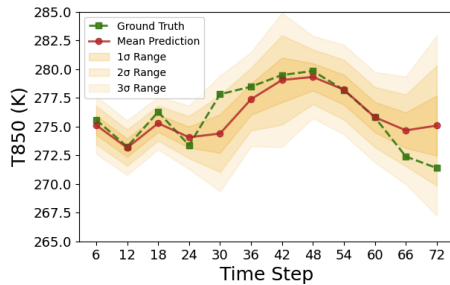


Figure 5: Forecast with confidence intervals.

Inference efficiency. Generally, numerical weather prediction models (e.g., IFS) require around 50 minutes for the medium-range global forecast, while deterministic ML weather prediction models take less than 1 minute (Rasp et al., 2020) but cannot model the weather uncertainty. CoDiCast needs about 3.6 minutes (see the last row in Table 2) for the global weather forecast, potentially balancing the efficiency and accuracy with essential uncertainty quantification. The efficiency also depends on the model complexity.

4.4 QUALITATIVE EVALUATION

In Figure 6, we qualitatively evaluate the performance of CoDiCast on global forecasting tasks for all target variables, Z500, T850, T2m, U10 and V10 at the lead time of 6 hours. The first row is the ground truth of the target variable, the second row is the prediction and the last row is the difference between the model prediction and the ground truth. From the scale of their color bars, we can tell that the error percentage is less than 3% for variables Z500, T850, and T2m. Nevertheless, error percentages over 50% exist for U10 and V10 even though only a few of them exist. Furthermore, we observe that most higher errors appear in the high-latitude ocean areas, probably due to the sparse data nearby. We provide visualizations for longer lead times (up to 3 days) in Appendix E.

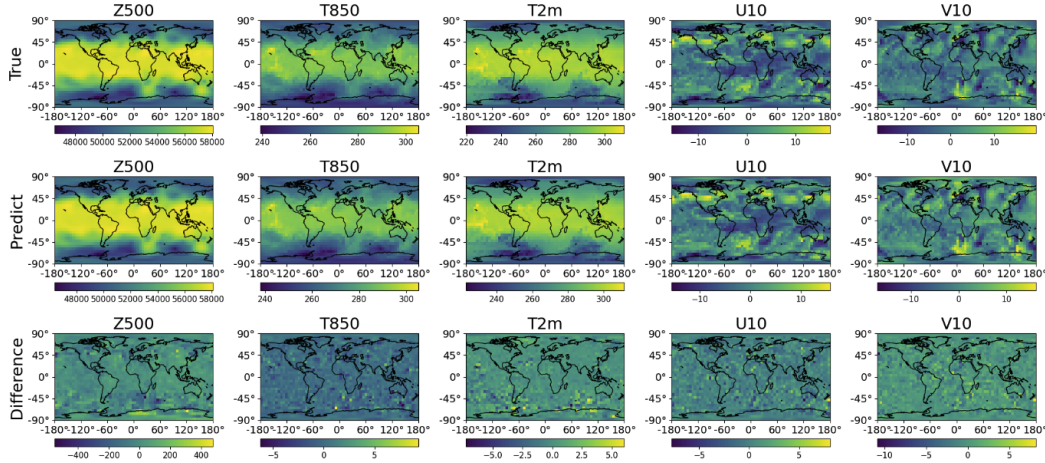


Figure 6: Visualization of true and predicted values at 6 hours lead time.

4.5 ABLATION STUDY

CoDiCast includes two important components: *pre-trained encoder* and *cross attention*. To study their effectiveness, we conduct an ablation study: (a) **No-encoder** directly considers past observations as conditions to diffusion model; (b) **No-cross-attention** simply concatenate the embedding and the noisy sample at each denoising step; (c) **No-encoder-cross-attention** concatenate the past observations and the noisy sample at each denoising step. Figure 7 shows the full CoDiCast consistently outperforms all other variants, verifying positive contributions of both components.

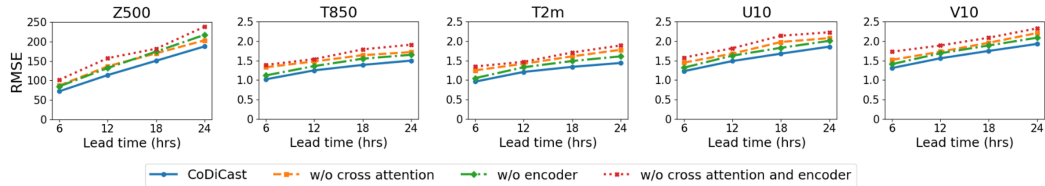


Figure 7: Ablation study to study the effect of pre-trained encoder and cross-attention.

4.6 PARAMETER STUDY

Diffusion step. We try various diffusion steps $N = \{250, 500, 750, 1000, 1500, 2000\}$. Table 2 shows that the accuracy improves as the number of diffusion steps increases when $N < 1000$, indicating that more intermediate steps are more effective in learning the imperceptible attributes during the denoising process. However, when $1000 < N < 2000$, the accuracy remains approximately flat but the inference time keeps increasing linearly. Considering the trade-off between accuracy and efficiency, we finally set $N = 1000$ for all experiments.

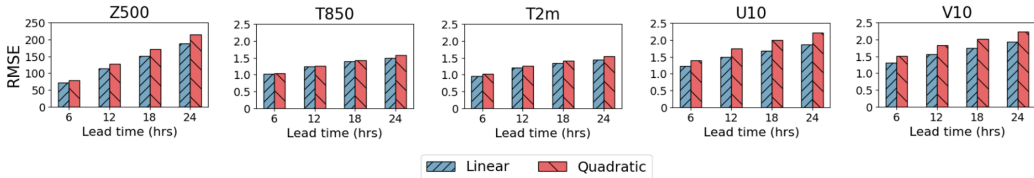


Figure 8: Effect of linear and quadratic variance scheduling methods.

Method for variance scheduling. We use the same start and end variance value, β , as DDPM (Ho et al., 2020) where $\beta \in [0.0001, 0.02]$. We study the effect of “linear” and “quadratic” variance scheduling in this section. The results are provided in Figure 8. It shows that the “linear” variance scheduling provides better performance than “quadratic” one for variables Z500, T2m, U10, and V10, while the performance of both “linear” and “quadratic” modes is roughly same for variable T850.

Table 2: Latitude-weighted RMSE with various diffusion steps. We mark the lowest scores in bold font. The last row represents the inference time of CoDiCast.

Variable	Lead	Diffusion Step					
		250	500	750	1000	1500	2000
Z500	24	696.1	324.8	190.6	186.5	193.5	191.9
T850	24	3.88	2.38	1.53	1.52	1.56	1.58
T2m	24	5.26	2.79	1.63	1.44	1.50	1.53
U10	24	2.74	2.05	1.81	1.87	1.99	2.01
V10	24	2.43	2.11	1.89	1.94	2.04	2.06
Inference time (min)		~ 3	~ 6	~ 10	~ 12	~ 20	~ 27

5 RELATED WORK

Physics-based Numerical Weather Prediction. Numerical Weather Prediction (NWP) methods achieve weather forecasts by modeling the system of the atmosphere, land, and ocean with complex differential equations (Bauer et al., 2015). For example, High-Resolution Forecasts System (HRES) (ECMWF, 2023) forecasts possible weather evolution out to 10 days ahead. However, it is a deterministic NWP method that only provides a single forecast. To overcome the limitation of deterministic methods, the ensemble forecast suite (ENS) (Buizza, 2008) was developed as an ensemble of 51 forecasts by the European Centre for Medium-Range Weather Forecasts (ECMWF). ENS provides a range of possible future weather states, allowing for investigation of the detail and uncertainty in the forecast. Even if NWP ensemble forecasts effectively model the weather evolution, they exhibit sensitivity to structural discrepancies across models and high computational demands (Balaji et al., 2022).

ML-Based Weather Prediction. Pangu (Bi et al., 2023) employed three-dimensional transformer networks and Earth-specific priors to deal with complex patterns in weather data. GraphCast (Lam et al., 2023) achieved medium-range weather prediction by utilizing an “encode-process-decode” configuration with each part implemented by graph neural networks (GNNs). GNNs perform effectively in capturing the complex relationship between a set of surface and atmospheric variables. A similar GNN-based work is (Keisler, 2022). Fuxi (Chen et al., 2023b) and Fengwu (Chen et al., 2023a) also employ the “encode-decode” strategy but with the transformer-based backbone. Four-CastNet (Pathak et al., 2022) applied Vision Transformer (ViT) and Adaptive Fourier Neural Operators (AFNO), while ClimaX (Nguyen et al., 2023) also uses a ViT backbone but the trained model can be fine-tuned to various downstream tasks. However, these models fall short in modeling the uncertainty of weather evolution (Jaseena & Kovoor, 2022) even though perturbations are added to initial conditions (Bülte et al., 2024) and dropout methods (Gal & Ghahramani, 2016) are used to mimic the uncertainty. Additionally, ClimODE (Verma et al., 2024) incorporated the physical knowledge and developed a continuous-time neural advection PDE weather model.

Diffusion Models. Diffusion models (Ho et al., 2020) have shown their strong capability in computer vision tasks, including image generation (Li et al., 2022), image editing (Nichol et al., 2021), semantic segmentation (Brempong et al., 2022) and point cloud completion (Luo & Hu, 2021). Conditional diffusion models (Ho & Salimans, 2022) were later proposed to make the generation step conditioned on the current context or situation. However, not many efforts have adopted diffusion models in global medium-range weather forecasting. More recent research has focused on

precipitation nowcasting (Asperti et al., 2023; Gao et al., 2024), and are localized in their predictions. GenCast (Price et al., May 2024) is a recently proposed conditional diffusion-based ensemble forecasting for medium-range weather prediction. However, their conditioning is to directly use the observations from the recent past, which is shown to be insufficient (see results in ablation study).

6 CONCLUSIONS

In this work, we start with analyzing the limitations of current deterministic numerical weather prediction (NWP) and machine-learning weather prediction (MLWP) approaches—they either cause substantial computational cost or lack uncertainty quantification in the forecasts. To address these limitations, we propose a conditional diffusion model, CoDiCast, which contains a conditional *pre-trained encoder* and a *cross-attention* component. Quantitative and qualitative experimental results demonstrate it can simultaneously complete more accurate predictions than existing MLWP-based models and a faster inference than NWP-based models while being capable of providing uncertainty quantification compared to deterministic methods. In conclusion, our model offers three key characteristics at the same time.

Limitation and Future work. We use low-resolution (5.625°) data currently due to the relatively slow inference process of diffusion models compared to deterministic ML models. In the future, we will focus on accelerating diffusion models (Song et al., 2020) to adapt the higher-resolution data. Besides the meteorological numerical data, weather events are often recorded or reported in the form of text. We will study how to leverage LLMs to extract their implicit interactions (Li et al., 2024) and inject them into diffusion models to guide the generation process.

ACKNOWLEDGMENTS

This work is supported by the Institute for Geospatial Understanding through an Integrative Discovery Environment (I-GUIDE), which is funded by the National Science Foundation (NSF) under award number: 2118329. Any opinions, findings, conclusions, or recommendations expressed herein are those of the authors and do not necessarily represent the views of NSF.

REFERENCES

- Peshawa Jamal Muhammad Ali, Rezhna Hassan Faraj, Erbil Koya, Peshawa J Muhammad Ali, and Rezhna H Faraj. Data normalization and standardization: a technical report. *Mach Learn Tech Rep*, 1(1):1–6, 2014.
- Andrea Asperti, Fabio Merizzi, Alberto Paparella, Giorgio Pedrazzi, Matteo Angelinelli, and Stefano Colamonaco. Precipitation nowcasting with generative diffusion models. *arXiv preprint arXiv:2308.06733*, 2023.
- V Balaji, Fleur Couvreur, Julie Deshayes, Jacques Gautrais, Frédéric Hourdin, and Catherine Rio. Are general circulation models obsolete? *Proceedings of the National Academy of Sciences*, 119(47):e2202075119, 2022.
- Pierre Baldi. Autoencoders, unsupervised learning, and deep architectures. In *Proceedings of ICML workshop on unsupervised and transfer learning*, pp. 37–49, Edinburgh, Scotland, 2012. JMLR Workshop and Conference Proceedings.
- Peter Bauer, Alan Thorpe, and Gilbert Brunet. The quiet revolution of numerical weather prediction. *Nature*, 525(7567):47–55, 2015.
- Zied Ben Bouallègue, Mariana CA Clare, Linus Magnusson, Estibaliz Gascon, Michael Maier-Gerber, Martin Janoušek, Mark Rodwell, Florian Pinault, Jesper S Dramsch, Simon TK Lang, et al. The rise of data-driven weather forecasting: A first statistical assessment of machine learning-based weather forecasts in an operational-like context. *Bulletin of the American Meteorological Society*, 105(6):E864–E883, 2024.
- Kaifeng Bi, Lingxi Xie, Hengheng Zhang, Xin Chen, Xiaotao Gu, and Qi Tian. Accurate medium-range global weather forecasting with 3d neural networks. *Nature*, 619(7970):533–538, 2023.

- Emmanuel Asiedu Brempong, Simon Kornblith, Ting Chen, Niki Parmar, Matthias Minderer, and Mohammad Norouzi. Denoising pretraining for semantic segmentation. In *Proceedings of the IEEE/CVF conference on computer vision and pattern recognition*, pp. 4175–4186, 2022.
- Roberto Buizza. Comparison of a 51-member low-resolution (t1399l62) ensemble with a 6-member high-resolution (t1799l91) lagged-forecast ensemble. *Monthly weather review*, 136(9):3343–3362, 2008.
- Christopher Bülte, Nina Horat, Julian Quinting, and Sebastian Lerch. Uncertainty quantification for data-driven weather models. *arXiv preprint arXiv:2403.13458*, 2024.
- Kang Chen, Tao Han, Junchao Gong, Lei Bai, Fenghua Ling, Jing-Jia Luo, Xi Chen, Leiming Ma, Tianning Zhang, Rui Su, et al. Fengwu: Pushing the skillful global medium-range weather forecast beyond 10 days lead. *arXiv preprint arXiv:2304.02948*, 2023a.
- Lei Chen, Xiaohui Zhong, Feng Zhang, Yuan Cheng, Yinghui Xu, Yuan Qi, and Hao Li. Fuxi: A cascade machine learning forecasting system for 15-day global weather forecast. *npj Climate and Atmospheric Science*, 6(1):190, 2023b.
- Ricky TQ Chen, Yulia Rubanova, Jesse Bettencourt, and David K Duvenaud. Neural ordinary differential equations. *Advances in neural information processing systems*, 31, 2018.
- ECMWF. Medium-range forecasts, 2023. URL <https://www.ecmwf.int/en/forecasts/documentation-and-support/medium-range-forecasts>.
- Yarin Gal and Zoubin Ghahramani. Dropout as a bayesian approximation: Representing model uncertainty in deep learning. In *international conference on machine learning*, pp. 1050–1059. PMLR, 2016.
- Zhihan Gao, Xingjian Shi, Boran Han, Hao Wang, Xiaoyong Jin, Danielle Maddix, Yi Zhu, Mu Li, and Yuyang Bernie Wang. Prediff: Precipitation nowcasting with latent diffusion models. *Advances in Neural Information Processing Systems*, 36, 2024.
- Kaiming He, Xiangyu Zhang, Shaoqing Ren, and Jian Sun. Deep residual learning for image recognition. In *Proceedings of the IEEE conference on computer vision and pattern recognition*, pp. 770–778, Las Vegas, Nevada, USA, 2016. Computer Vision Foundation.
- Hans Hersbach, Bill Bell, Paul Berrisford, Shoji Hirahara, András Horányi, Joaquín Muñoz-Sabater, Julien Nicolas, Carole Peubey, Raluca Radu, Dinand Schepers, et al. The era5 global reanalysis. *Quarterly Journal of the Royal Meteorological Society*, 146(730):1999–2049, 2020.
- Amir Hertz, Ron Mokady, Jay Tenenbaum, Kfir Aberman, Yael Pritch, and Daniel Cohen-Or. Prompt-to-prompt image editing with cross attention control. *arXiv preprint arXiv:2208.01626*, 2022.
- Pradeep Hewage, Marcello Trovati, Ella Pereira, and Ardhendu Behera. Deep learning-based effective fine-grained weather forecasting model. *Pattern Analysis and Applications*, 24(1):343–366, 2021.
- Jonathan Ho and Tim Salimans. Classifier-free diffusion guidance. *arXiv preprint arXiv:2207.12598*, 2022.
- Jonathan Ho, Ajay Jain, and Pieter Abbeel. Denoising diffusion probabilistic models. *Advances in neural information processing systems*, 33:6840–6851, 2020.
- KU Jaseena and Binsu C Koor. Deterministic weather forecasting models based on intelligent predictors: A survey. *Journal of king saud university-computer and information sciences*, 34(6): 3393–3412, 2022.
- Ryan Keisler. Forecasting global weather with graph neural networks. *arXiv preprint arXiv:2202.07575*, 2022.
- Dmitrii Kochkov, Janni Yuval, Ian Langmore, Peter Norgaard, Jamie Smith, Griffin Mooers, Milan Klöwer, James Lottes, Stephan Rasp, Peter Düben, et al. Neural general circulation models for weather and climate. *Nature*, pp. 1–7, 2024.

- Remi Lam, Alvaro Sanchez-Gonzalez, Matthew Willson, Peter Wirnsberger, Meire Fortunato, Ferran Alet, Suman Ravuri, Timo Ewalds, Zach Eaton-Rosen, Weihua Hu, et al. Learning skillful medium-range global weather forecasting. *Science*, 382(6677):1416–1421, 2023.
- Jussi Leinonen, Ulrich Hamann, Daniele Nerini, Urs Germann, and Gabriele Franch. Latent diffusion models for generative precipitation nowcasting with accurate uncertainty quantification. *arXiv preprint arXiv:2304.12891*, 2023.
- Haobo Li, Zhaowei Wang, Jiachen Wang, Alexis Kai Hon Lau, and Huamin Qu. Cllmate: A multi-modal llm for weather and climate events forecasting. *arXiv preprint arXiv:2409.19058*, 2024.
- Haoying Li, Yifan Yang, Meng Chang, Shiqi Chen, Huajun Feng, Zhihai Xu, Qi Li, and Yueting Chen. Srdiff: Single image super-resolution with diffusion probabilistic models. *Neurocomputing*, 479:47–59, 2022.
- Shitong Luo and Wei Hu. Diffusion probabilistic models for 3d point cloud generation. In *Proceedings of the IEEE/CVF conference on computer vision and pattern recognition*, pp. 2837–2845, 2021.
- Bruno Merz, Christian Kuhlicke, Michael Kunz, Massimiliano Pittore, Andrey Babeyko, David N Bresch, Daniela IV Domeisen, Frauke Feser, Inga Koszalka, Heidi Kreibich, et al. Impact forecasting to support emergency management of natural hazards. *Reviews of Geophysics*, 58(4): e2020RG000704, 2020.
- SK Morley, DT Welling, and JR Woodroffe. Perturbed input ensemble modeling with the space weather modeling framework. *Space Weather*, 16(9):1330–1347, 2018.
- Tung Nguyen, Johannes Brandstetter, Ashish Kapoor, Jayesh K Gupta, and Aditya Grover. Climax: A foundation model for weather and climate. *arXiv preprint arXiv:2301.10343*, 2023.
- Alex Nichol, Prafulla Dhariwal, Aditya Ramesh, Pranav Shyam, Pamela Mishkin, Bob McGrew, Ilya Sutskever, and Mark Chen. Glide: Towards photorealistic image generation and editing with text-guided diffusion models. *arXiv preprint arXiv:2112.10741*, 2021.
- Tim Palmer. The ecmwf ensemble prediction system: Looking back (more than) 25 years and projecting forward 25 years. *Quarterly Journal of the Royal Meteorological Society*, 145:12–24, 2019.
- TN Palmer. Towards the probabilistic earth-system simulator: A vision for the future of climate and weather prediction. *Quarterly Journal of the Royal Meteorological Society*, 138(665):841–861, 2012.
- Jaideep Pathak, Shashank Subramanian, Peter Harrington, Sanjeev Raja, Ashesh Chattopadhyay, Morteza Mardani, Thorsten Kurth, David Hall, Zongyi Li, Kamyar Azizzadenesheli, et al. Four-castnet: A global data-driven high-resolution weather model using adaptive fourier neural operators. *arXiv preprint arXiv:2202.11214*, 2022.
- Ilan Price, Alvaro Sanchez-Gonzalez, Ferran Alet, Timo Ewalds, Andrew El-Kadi, Jacklynn Stott, Shakir Mohamed, Peter Battaglia, Remi Lam, and Matthew Willson. Gencast: Diffusion-based ensemble forecasting for medium-range weather. *arXiv preprint arXiv:2312.15796*, May 2024.
- Stephan Rasp, Peter D Dueben, Sebastian Scher, Jonathan A Weyn, Soukayna Mouatadid, and Nils Thuerey. Weatherbench: a benchmark data set for data-driven weather forecasting. *Journal of Advances in Modeling Earth Systems*, 12(11):e2020MS002203, 2020.
- MJ Rodwell and TN Palmer. Using numerical weather prediction to assess climate models. *Quarterly Journal of the Royal Meteorological Society: A journal of the atmospheric sciences, applied meteorology and physical oceanography*, 133(622):129–146, 2007.
- Robin Rombach, Andreas Blattmann, Dominik Lorenz, Patrick Esser, and Björn Ommer. High-resolution image synthesis with latent diffusion models. In *Proceedings of the IEEE/CVF conference on computer vision and pattern recognition*, pp. 10684–10695, 2022.

- Olaf Ronneberger, Philipp Fischer, and Thomas Brox. U-net: Convolutional networks for biomedical image segmentation. In *Medical image computing and computer-assisted intervention—MICCAI 2015: 18th international conference, October 5-9, 2015, proceedings, part III 18*, pp. 234–241, 2015.
- Jimeng Shi, Rukmangadh Myana, Vitalii Stebliankin, Azam Shirali, and Giri Narasimhan. Explainable parallel rnn with novel feature representation for time series forecasting. In *International Workshop on Advanced Analytics and Learning on Temporal Data*, pp. 56–75, Torino, Italy, 2023. Springer.
- Jimeng Shi, Zeda Yin, Arturo Leon, Jayantha Obeysekera, and Giri Narasimhan. Fidlar: Forecast-informed deep learning architecture for flood mitigation. *arXiv preprint arXiv:2402.13371*, 2024.
- Talha Siddique, Md Shaad Mahmud, Amy M Keese, Chigomezzyo M Ngwira, and Hyunju Connor. A survey of uncertainty quantification in machine learning for space weather prediction. *Geosciences*, 12(1):27, 2022.
- Julia Slingo and Tim Palmer. Uncertainty in weather and climate prediction. *Philosophical Transactions of the Royal Society A: Mathematical, Physical and Engineering Sciences*, 369(1956): 4751–4767, 2011.
- Jiaming Song, Chenlin Meng, and Stefano Ermon. Denoising diffusion implicit models. *arXiv preprint arXiv:2010.02502*, 2020.
- Ashish Vaswani, Noam Shazeer, Niki Parmar, Jakob Uszkoreit, Llion Jones, Aidan N Gomez, Łukasz Kaiser, and Illia Polosukhin. Attention is all you need. In *Advances in Neural Information Processing Systems*, volume 30, Long Beach, CA, USA, 2017. Curran Associates Inc.
- Yogesh Verma, Markus Heinonen, and Vikas Garg. Climode: Climate and weather forecasting with physics-informed neural odes. *arXiv preprint arXiv:2404.10024*, 2024.
- Lvmin Zhang, Anyi Rao, and Maneesh Agrawala. Adding conditional control to text-to-image diffusion models. In *Proceedings of the IEEE/CVF International Conference on Computer Vision*, pp. 3836–3847, 2023.

APPENDIX

A DATASET

We introduce a detailed description of the ERA5 dataset. As the predominant data source for learning and benchmarking weather prediction systems, the ERA5 reanalysis archive from the European Center for Medium-Range Weather Forecasting (ECMWF) provides reanalyzed data from 1979 onwards. This data is available on a $0.25^\circ \times 0.25^\circ$ global latitude-longitude grid of the Earth’s sphere, at hourly intervals, with different atmospheric variables at 37 different altitude levels and some variables on the Earth’s surface. The grid overall contains 721×1440 grid points for latitude and longitude, respectively. Due to the limited computational resources, we used the preprocessed version of ERA5 from WeatherBench (Rasp et al., 2020) in our work. This dataset¹ contains re-gridded ERA5 reanalysis data in three lower resolutions: 5.625° , 2.8125° , and 1.40625° . To guarantee fair comparison with the benchmarks (Verma et al., 2024), we follow the ClimODE work and choose the 5.625° resolution dataset for variables: geopotential at 500 hPa pressure level (Z500), atmospheric temperature at 850 hPa pressure level (T850), ground temperature (T2m), 10 meter U wind component (U10) and 10 meter V wind component (V10). *Single* represents surface-level variables, and *Atmospheric* represents time-varying atmospheric properties at chosen altitudes. A sample at a certain time point can be represented by $X^t \in \mathbb{R}^{H \times W \times C}$ where $H \times W$ refers to the spatial resolution of data which depends on how densely we grid the globe over latitude and longitude. C refers to the number of channels (i.e. weather variables). In our work, H, W , and C are 32, 64, and 5, accordingly. Notably, both Z500 and T850 are two popular verification variables for global weather prediction models, while T2m, U10, and V10 directly pertain to human activities.

Table 3: Variable Information.

Type	Variable	Abbrev.	ECMWF ID	Levels	Range	Unit
Single	2 metre temperature	T2m	167		[193.1, 323.6]	K
Single	10 metre U wind	U10	165		[-37.3, 30.2]	m/s
Single	10 metre V wind	V10	166		[-31.5, 32.5]	m/s
Atmospheric	Geopotential	Z	129	500	[43403.6, 59196.9]	m^2/s^2
Atmospheric	Temperature	T	130	850	[217.9, 313.3]	K

B MODEL ARCHITECTURE

We present the detailed architectures of the autoencoder, cross-attention block, and U-Net model used in our work. Meanwhile, we also illustrate how we organize the input data and how they flow through different machine-learning model blocks. We recommend readers check out Figures 2, 3, and 4 while looking into the following architectures.

B.1 AUTOENCODER

We train an autoencoder model consisting of two main parts: an encoder and a decoder. The encoder compresses the input to feature representation (embedding) in the latent space. The decoder reconstructs the input from the latent space. After training, the pre-trained encoder can be extracted to generate embedding for input data. In our work, the convolutional autoencoder architecture is designed for processing spatiotemporal weather data at a time point, t , represented as $X^t \in \mathbb{R}^{H \times W \times C}$. The encoder consists of a series of convolutional layers with 2×2 filters, each followed by a ReLU activation function. The layers have 32, 128, 256, and 512 filters, respectively, allowing for a progressive increase in feature depth, thereby capturing essential patterns in the data. The decoder starts with 512 filters and reduces the feature depth through layers with 256 and 128 filters, each followed by ReLU activations. This design ensures the reconstruction of the input data while preserving the learned features, enabling the model to extract meaningful embeddings that encapsulate the spatiotemporal characteristics of the input.

¹<https://github.com/pangeo-data/WeatherBench>

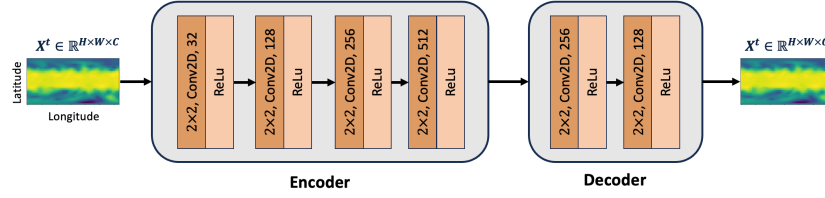


Figure 9: Architecture of the Autoencoder model.

B.2 CROSS-ATTENTION

The cross-attention is used to learn the interaction between past observations and the noisy data at each diffusion step. We consider the past observations as the conditions to guide the diffusion models during generation. Given the weather states in the past two time points, $X^{T \times H \times W \times C}$, we utilize the pre-trained encoder to learn the embedding from each time point, $X^{T \times H \times W \times d_e}$. To better use the *attention* mechanism, we first reshape it to $X^{(H \times W) \times (T \times d_e)}$ and convert it to key and value matrices: $K \in \mathbb{R}^{(H \times W) \times d_k}$ and $V \in \mathbb{R}^{(H \times W) \times d_v}$. We consider the noisy sample at each diffusion step, $X_n \in \mathbb{R}^{T \times H \times W \times C}$, as a query. It is transformed to $Q \in \mathbb{R}^{(H \times W) \times d_q}$. Then, the *cross-attention* mechanism is implemented by $\text{Attention}(Q, K, V) = \text{softmax}\left(\frac{QK^T}{\sqrt{d}}\right) \cdot V$. In our work, we set $d_q = d_k = d_v = d = 64$ where d is the projection embedding length.

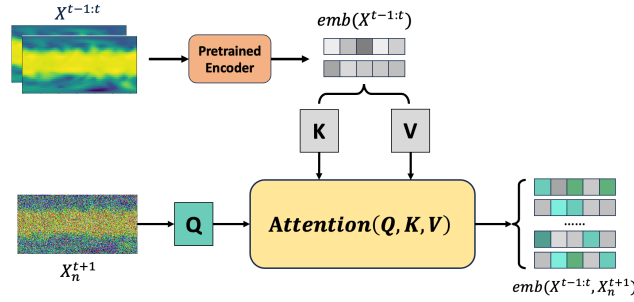


Figure 10: Architecture of the cross-attention block.

B.3 U-NET

Our U-Net architecture is similar to DDPM (Ho et al., 2020) but with necessary changes to adapt to the problems in this work. Each U-Net unit comprises two ResNet blocks (He et al., 2016) and a convolutional up/downsampling block. Self-attention was included between the convolution blocks once we reached a specific resolution ($4 \times 8, 2 \times 4$), represented in blue arrows. We employ four U-Net units for both the downsampling and upsampling processes. We use *MaxPooling* in the downsampling units where the channel dimension is $64 \times j$ ($j = \{1, 2, 3, 4\}$ refers to the layer index). The upsampling units follow the reverse order. We set the upsampling factor as 2 and the “nearest” interpolation. We used the *swish* activation function throughout the network. We also had *GroupNormalization* layer for more stable training where the number of groups for *Group Normalization* is 8. *Group Normalization* divides the channels into groups and computes within each group the mean and variance for normalization.

Notably, for the target variable, X^{t+1} at the n diffusion step, the input to U-Net involves the mixture embedding of past weather states, $X^{t-1:t}$, and the noisy sample from the last diffusion step, X_n^{t+1} . The mixture embedding is obtained by the cross-attention mechanism described above. The channel dimension output is five because of five weather variables of interest to predict. This is achieved by a convolutional layer with a 1×1 kernel.

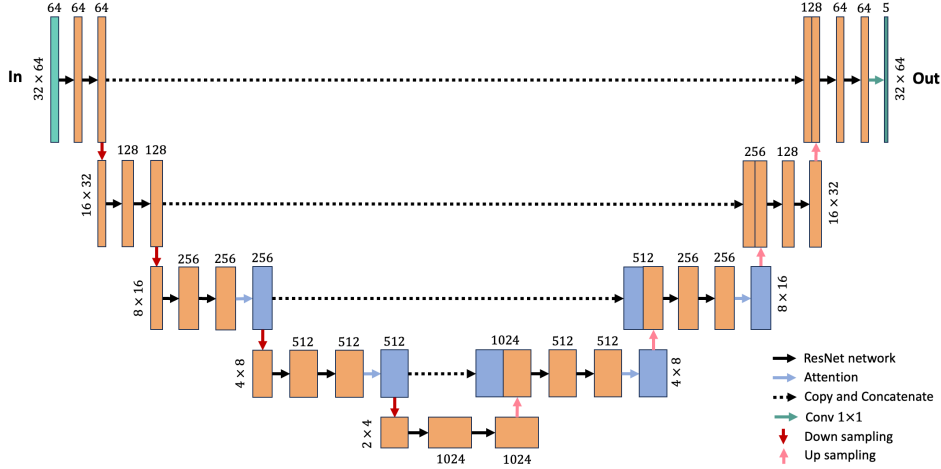


Figure 11: Architecture of the U-Net model.

C TRAINING DETAILS

We provide the hyperparameters for training our model `CoDiCast`, which includes pre-training `Autoencoder` and training the `denoiser` network. Since it is more helpful to find the minimum loss if using a decayed learning rate as the training progresses, we applied an exponential decay function to an optimizer step given a provided initial learning rate.

Table 4: Hyperparameters of Training Autoencoder.

Abbreviation	Training Autoencoder	Training Denoiser
Epochs	100	800
Batch_size	128	256
Learning_rate	1e-4	2e-4
Decay_steps	10000	10000
Decay_rate	0.95	0.95

D EVALUATION METRICS

Root Mean Square Error. Following (Verma et al., 2024), we assess the model performance using latitude-weighted Root Mean Square Error (RMSE). RMSE measures the average difference between values predicted by a model and the actual values.

$$\text{RMSE} = \frac{1}{M} \sum_{m=1}^M \sqrt{\frac{1}{H \times W} \sum_{h=1}^H \sum_{w=1}^W L(h) (\tilde{X}_{m,h,w} - X_{m,h,w})^2},$$

where $L(h) = \frac{1}{H} \cos(h) \sum_{h'}^H \cos(h')$ is the latitude weight and M represents the number of test samples.

Anomaly Correlation Coefficient. ACC is the correlation between prediction anomalies \tilde{X}' relative to climatology and ground truth anomalies \tilde{X} relative to climatology. ACC is a critical metric in climate science to evaluate the model's performance in capturing unusual weather or climate events.

$$\text{ACC} = \frac{\sum_{m,h,w} L(h) \tilde{X}'_{m,h,w} X'_{m,h,w}}{\sqrt{\sum_{m,h,w} L(h) \tilde{X}'_{m,h,w}^2 \cdot \sum_{m,h,w} L(h) X'_{m,h,w}^2}},$$

where observed and forecasted anomalies $X' = X - C$, $\tilde{X}' = \tilde{X} - C$, and climatology $C = \frac{1}{M} \sum_m X$ is the temporal mean of the ground truth data over the entire test set.

E VISUALIZING PREDICTION WITH LONGER LEAD TIMES

We provide the forecast at longer lead times (i.e., 24, 48, 72, 144 hours). The first row is the ground truth of the target variable, the second row is the prediction of CoDiCast and the last row is the difference between the model prediction and the ground truth.

E.1 SHORT RANGE WEATHER FORECASTING

Short-range weather forecasting at the 24-hour lead time for all target variables.

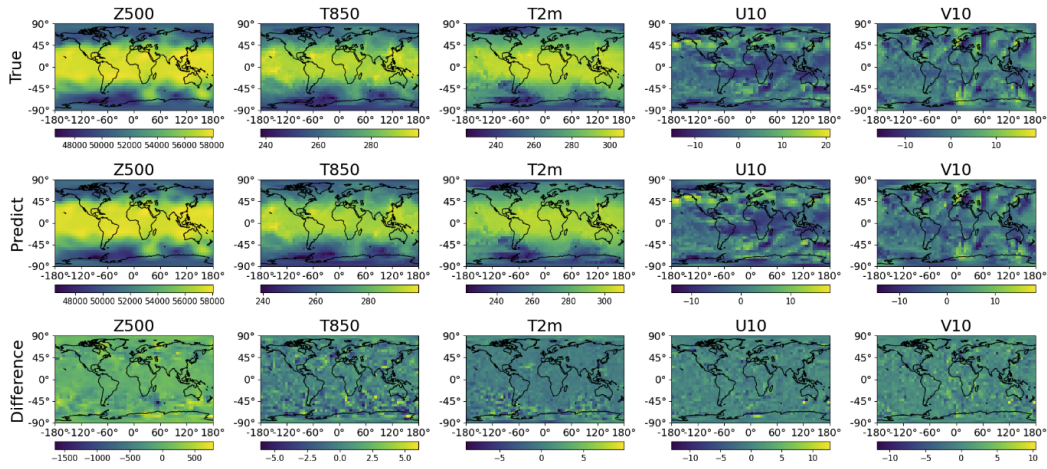


Figure 12: Visualizations of true and predicted values of all five variables at 24 hours lead time.

E.2 MEDIUM-RANGE WEATHER FORECASTING

Medium-range weather forecasting at the 48-hour lead time for all target variables.

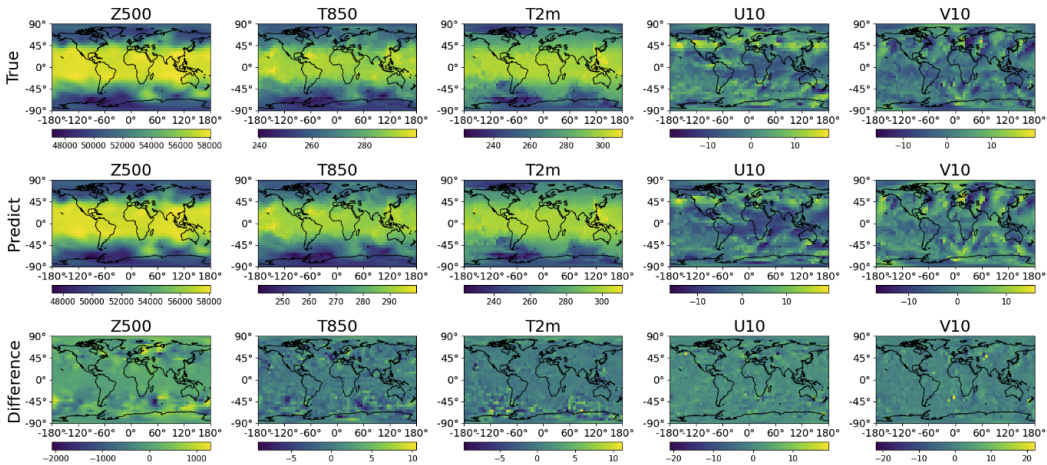


Figure 13: Visualizations of true and predicted values of all five variables at 48 hours lead time.

E.3 MEDIUM-RANGE WEATHER FORECASTING

Longer-range weather forecasting at the 72-hour lead time for all target variables.

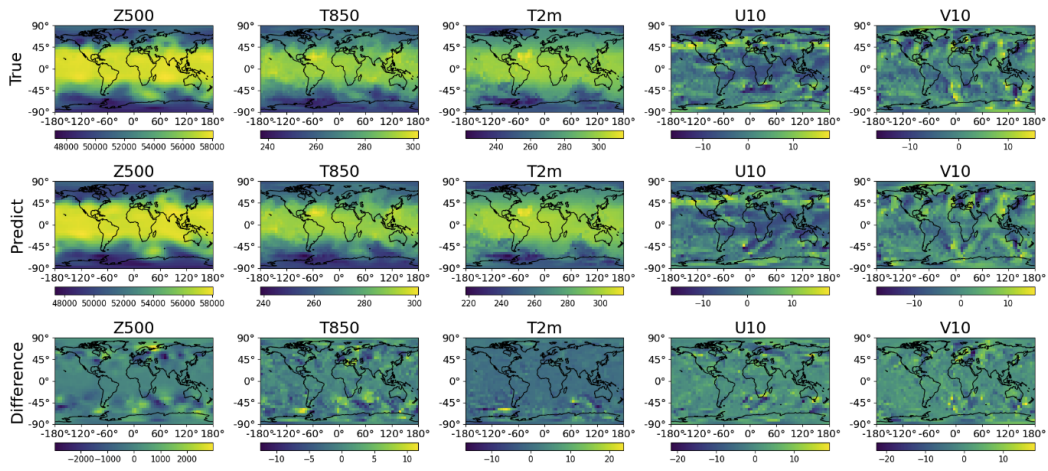


Figure 14: Visualizations of true and predicted values of all five variables at 72 hours lead time.

E.4 LONG-RANGE WEATHER FORECASTING

Longer-range weather forecasting at the 144-hour lead time for all target variables.

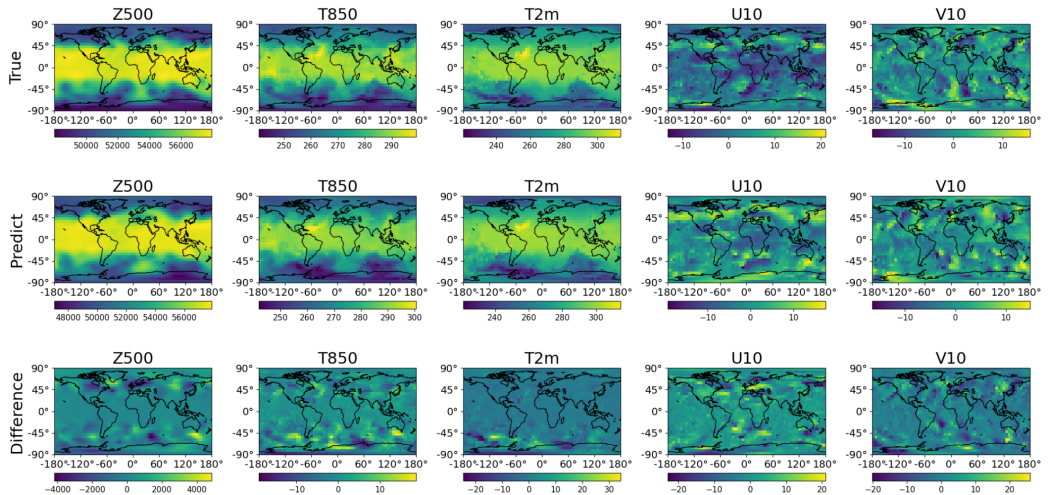


Figure 15: Visualizations of true and predicted values of all five variables at 144 hours lead time.